International Journal of Remote Sensing, 2013
Vol. 34, No. 20, 7178–7198, http://dx.doi.org/10.1080/01431161.2013.817716

Taylor & Francis
Taylor & Francis Group

Remote sensing and geologic mapping of glaciovolcanic deposits in the region surrounding Askja (Dyngjufjöll) volcano, Iceland

A.H. Graettinger[a]*, M.K. Ellis[a], I.P. Skilling[b], K. Reath[a], M.S. Ramsey[a], R.J. Lee[a], C.G. Hughes[c], and D.W. McGarvie[d]

[a]*Department of Geology and Planetary Science, University of Pittsburgh, Pittsburgh, PA, USA;* [b]*Energy and Environment Research Institute, University of South Wales, Pontypridd, UK;* [c]*Earth Surface Science, JPL, Pasadena, CA, USA;* [d]*Department of Environment, Earth and Ecosystems, The Open University, Edinburgh, UK*

(*Received 23 February 2013; accepted 28 May 2013*)

Downloaded by [Michael Ramsey] at 16:35 18 July 2013

The surface geology of the Northern Volcanic Zone in Iceland is dominated by volcanic ridges, central volcanoes, shield volcanoes, and tuyas. The largest features are typically ice-confined (glaciovolcanic) in origin, and are overlain by voluminous Holocene (subaerial) lavas and glacial outwash deposits. The literature has focused heavily on prominent or very young features, neglecting small and older volcanic features. The purpose of this study is to demonstrate the application of remote-sensing mapping techniques to the glaciovolcanic environment in order to identify dominant lithologies and determine locations for textural, stratigraphic, and age studies. The deposits targeted in this study occur on and around Askja volcano, in central Iceland, including Pleistocene glaciovolcanic tuffs and subaerial pumice from the 1875 rhyolitic eruption of Askja. Data from the Advanced Spaceborne Thermal Emission and Reflection Radiometer (ASTER) were used in conjunction with previously published geologic and remote-sensing data sets and recent field work on glaciovolcanic deposits of Askja for validation. Remotely acquired data sets include aerial photographs and one ASTER scene obtained in August 2010. Visible and near-infrared (VNIR) and thermal infrared (TIR) classifications and linear deconvolution of the TIR emissivity data were performed using end-members derived from regions of interest and laboratory spectra. End-members were selected from samples of representative lithologic units within the field area, including glaciovolcanic deposits (pillow lavas, tuffs, etc.), historical deposits (1875 pumice, 1920s basaltic lavas), and Holocene basaltic lavas from Askja. The results demonstrate the potential for remote sensing-based ground cover mapping of areas of glaciovolcanic deposits relevant to palaeo-ice reconstructions in areas such as Iceland, Antarctica, and British Columbia. Remote sensing-based mapping will benefit glaciovolcanic studies, by determining the lithologic variability of these relatively inaccessible massifs and serving as an important springboard for the identification of future field sites in remote areas.

1. Introduction

The Icelandic landscape is dominated by basaltic Pleistocene glaciovolcanic and Holocene landforms. Rhyolitic deposits comprise approximately 1% of the total volume of volcanic

*Corresponding author. Present address: Center for Geohazard Studies, University at Buffalo, NY, USA. Email: agraettinger@gmail.com

© 2013 Taylor & Francis

deposits exposed in Iceland (Jakobsson, Jónasson, and Sigurdsson 2008). Simplified geologic maps exist for the entire country, with detailed studies of individual locations of interest. One area that has received considerable attention in the last century is Askja (Dyngjufjöll), a glaciovolcanic central volcano in the Northern Volcanic Zone (NVZ) (Figure 1). Central volcanoes, such as Askja, are basaltic shield volcanoes with intermittent rhyolitic activity, and typically display collapsed calderas. Central volcanoes are associated with long-term polygenetic growth occurring along the active and ancient rifts in Iceland. These massifs are typically dominated by glaciovolcanic deposits produced in and around ice-confined lakes. The resulting massifs are steep-sided constructs of pillow lavas, glassy ash, and lapilli tuff deposits. Locally emergent subaerial lavas cap glaciovolcanic deposits; these lavas were produced after the massif grew above water level, or through drainage of the surrounding lake. The relative proportions of these lithofacies at glaciovolcanic centres can vary dramatically from dominantly fragmental (i.e. Helgafell (Schopka, Gudmundsson, and Tuffen 2006)) to totally lava-dominated deposits (i.e. Undirhlíðar, Iceland, and Pillow Ridge, Canada (Edwards et al. 2009)) and varying combinations of the two (i.e. Herðubreið, Iceland (Werner, Schmincke, and Sigvaldason 1996)). The Askja complex is composed of a wide variety of fragmental and coherent glaciovolcanic and subaerial deposits bisected by at least three calderas, and is the site of recent effusive and explosive eruptions (1875, 1920–1929, and 1961) (Annertz, Nilsson, and Sigvaldason 1985). This area is of interest to volcanologists and palaeoclimate researchers due to its

Downloaded by [Michael Ramsey] at 16:35 18 July 2013

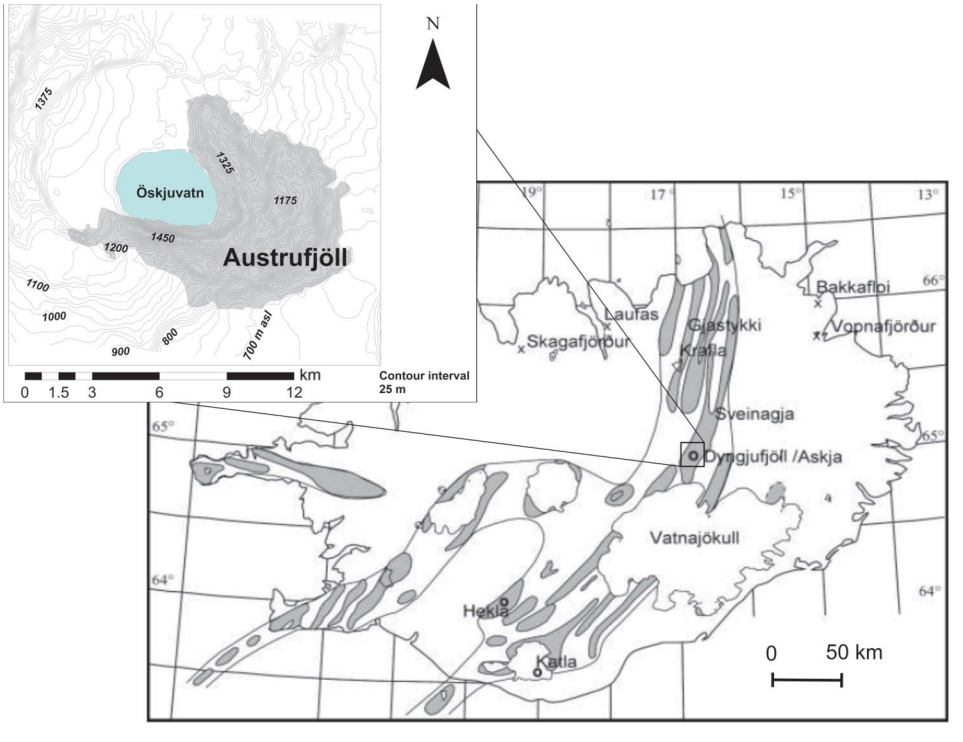

Figure 1. Location map of Iceland with the volcanic zones highlighted in grey (modified from Sigvaldason 2002).
Note: Askja is located just north of Vatnajökull ice cap. The Northern Volcanic Zone stretches north from the Vatnajökull icecap to the coast. Inset shows the Austurfjöll glaciovolcanic massif in relation to Öskjuvatn, the caldera lake of Askja.

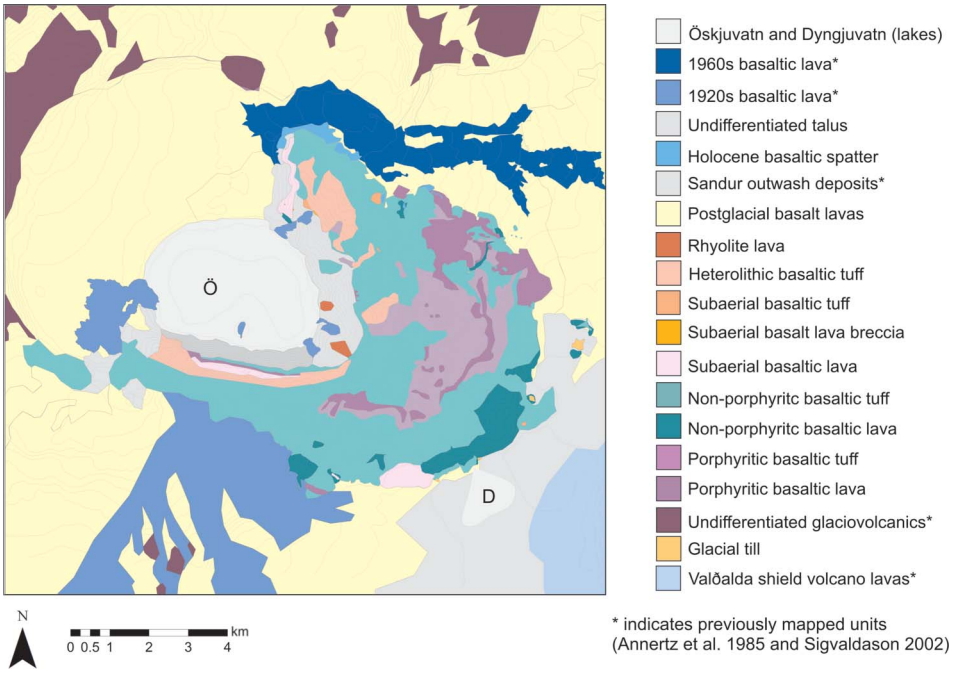

Figure 2. Geologic map of Austurfjöll glaciovolcanic sequences produced through field investigations during 2010–11 and surrounding simplified units mapped previously by Annertz, Nilsson, and Sigvaldason (1985) and Sigvaldason (2002). Talus includes some areas of undifferentiated deposits from the 1875 rhyolitic eruption.

range of basaltic to rhyolitic products and extended ice-confined eruptive history. The bulk of the research conducted on this volcano, however, has focused on its historic subaerial activity. Maps of the region group all of the local glaciovolcanic features into one ambiguous unit (Sigvaldason 2002). A field-based mapping project of the glaciovolcanic sequences of Askja's 49 km^2 eastern mountains (Austurfjöll) was conducted in 2010 and 2011 (Figure 2).

The work presented here uses the existing geologic data (recent and older maps) to validate a remote sensing-based mapping project of Askja and the surrounding region using a variety of satellite- and laboratory-acquired data. The primary input is an ASTER scene acquired in August 2010 and the ASTER global digital elevation model (GDEM). The remote sensing-based geologic map enabled the identification of large-scale lithologic variation within previously recognized, but unstudied, glaciovolcanic massifs near Askja. In particular, the identification of two major textural groups of glaciovolcanic deposits reveals the diversity in eruption styles of these centres in northern Iceland. Additionally, the work enabled the discrimination of the modern distribution of widespread, partially remobilized rhyolitic pyroclastic deposits which locally obscure older deposits. This project serves as a practical assessment of the use of remote sensing-based geologic mapping of typically inaccessible glaciovolcanic terrains such as Iceland, British Columbia, and Antarctica. Maps similar to the one produced in this study would be beneficial in regional comparison of glaciovolcanic deposit types (effusive coherent deposit-dominated, or more energetic explosive fragmental-dominated massifs). Such maps would also aid in the selection of field locations for stratigraphic and textural studies of these deposits, which are an invaluable palaeo-ice thickness proxy in dynamic environments such as Iceland.

Downloaded by [Michael Ramsey] at 16:35 18 July 2013

1.2. Details of study area

Askja is a large basalt-dominated central volcano around 40 km north of the modern Vatnajökull icecap (Figure 1). The major topographic feature of the volcano is a glaciovolcanic massif composed of Austurfjöll and Thorvaldstindur fissure ridges. The evolution of this massif consists of multiple eruptions of fissure-fed micro- and macro-porphyritic lavas, breccias, and tuffs (Figure 2). These deposits were mapped in part by Sigvaldason (1968, 2002) and in great detail by Graettinger (2012).

Maps of historical volcanic deposits from Askja and regional geologic features have been published in the last century (Thoroddsen 1925; Bemmelen and Rutten 1955; Thorarinsson and Sigvaldason 1962; Þorarinsson 1963; Sigvaldason 1968; Annertz, Nilsson, and Sigvaldason 1985; Sigvaldason 2002; Carey, Houghton, and Thordarson 2009; Hjartardóttir, Einarsson, and Sigurdsson 2009; Carey, Houghton, and Thordarson 2010). Additional information on the nature of the historic volcanic activity has been collected since 1875 following a 0.321 km^3 rhyolitic caldera-forming eruption from Askja (Sigvaldason 1964; Sigurdsson and Sparks 1978; Höskuldsson 1987; Sigvaldason 2002; Carey, Houghton, and Thordarson 2009; Carey, Houghton, and Thordarson 2010; Kuritani et al. 2011). Previously published maps used in this study include a lineament and simplified geology map (2400 km^2) (Hjartardóttir, Einarsson, and Sigurdsson 2009), and a map of the Holocene lavas surrounding Askja (1400 km^2) with some simplified units of glaciovolcanic and interglacial origin (Annertz, Nilsson, and Sigvaldason 1985). The stratigraphy of nearby glaciovolcanic edifice Herðubreið has also been described (Werner, Schmincke, and Sigvaldason 1996; Werner and Schmincke 1999). These data, in conjunction with new field evidence from Askja (Graettinger 2012), provide excellent opportunities to validate remotely collected data through comparison with samples and field observations (Figure 3). Other predominant features in this region include the glacial river, Jökulsá á Fjöllum, that flows roughly south–north along the eastern edge of the ASTER scene; Dyngjuvatn, a shallow periglacial lake between Askja and Valðalða (interglacial shield volcano); Öskjuvatn, a lake filling the youngest caldera of Askja; and extensive sandur (glacial outwash) plains derived from Vatnajökull.

Remote-sensing data include: aerial photographs collected by LoftMyndir Iceland comprising a greyscale mosaic in 2003 (850 km^2) and one orthorectified colour image in 2008 (50 km^2), and a DEM created by LoftMyndir Iceland from steropairs of orthophotos (280 km^2). A daytime ASTER scene acquired on 8 August 2010 (AST_L1A.003:2080525361) allowed the mapped area to be extended to approximately 4000 km^2. ASTER level 2 data used for this study include the atmospherically corrected surface radiance product (15 m/pixel for the visible and near-infrared (VNIR) and 90 m/pixel for TIR), the VNIR surface reflectance product (15 m/pixel), and the TIR surface emissivity product (90 m/pixel) (Figure 3). Unfortunately, shortwave infrared data from the ASTER instrument are not available for scenes collected after 2008 and this was the only clear daytime scene of the Askja volcano in the ASTER archive. The VNIR and TIR data were integrated with 25 m resolution ASTERGDEM, which encompasses all of the previously listed data sets.

2. Methodology

The creation of a 4000 km^2 ground cover map of Askja and its surroundings involved the use of VNIR and TIR laboratory hyperspectral data of rock samples, VNIR, and TIR multispectral data extracted from the ASTER data, topographic data (ASTERGDEM, AusturfjöllDEM), detailed (Figure 2) and simplified (Figure 3) geologic maps, as well as

Downloaded by [Michael Ramsey] at 16:35 18 July 2013

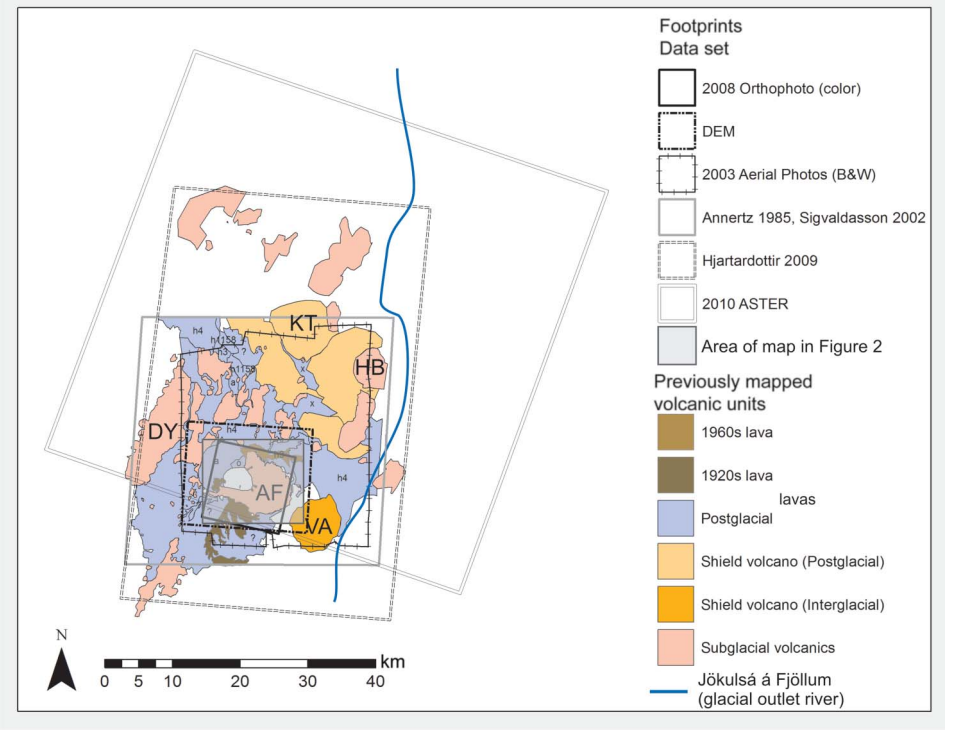

Figure 3. Regional geologic map compiled from previously published sources. Outlines indicate footprints of datasets used to compile the regional map and remote-sensing data sets utilized in this study. Abbreviations reference features that are discussed in detail in the text: DY, Dyngjufjöll Ytri; HB, Herðubreið; AF, Austurfjöll; VA, Valðalða; KT, Kollóttadyngja.

several different image-processing approaches using Environment for Visualizing Images (ENVI) software. It was through comparison and correlation of these varying spatial and spectral resolution data sets that the best-fit map (BFM) was produced. The steps used to produce the BFM are summarized in Figure 4.

2.1. Data collection

Remote-sensing data sets were augmented by the collection of lithologic and stratigraphic measurements from the field area. Field investigations resulted in the production of a lithofacies map of Austurfjöll massif and sample collection of representative surface units.

2.1.1. Field work

The surface volcanic geology of the area of interest was studied in detail through two field expeditions in 2010 and 2011 and analysis of aerial photographs. Representative samples of the dominant lithologies were identified on and around Austurfjöll in order to create a spectral end-member library. End-members were selected and sampled based on several criteria including: (1) their compositional relevance to the evolution of Askja massif (both basalts and rhyolite); (2) their abundance in the surrounding landscape (occurring over continuous

Downloaded by [Michael Ramsey] at 16:35 18 July 2013

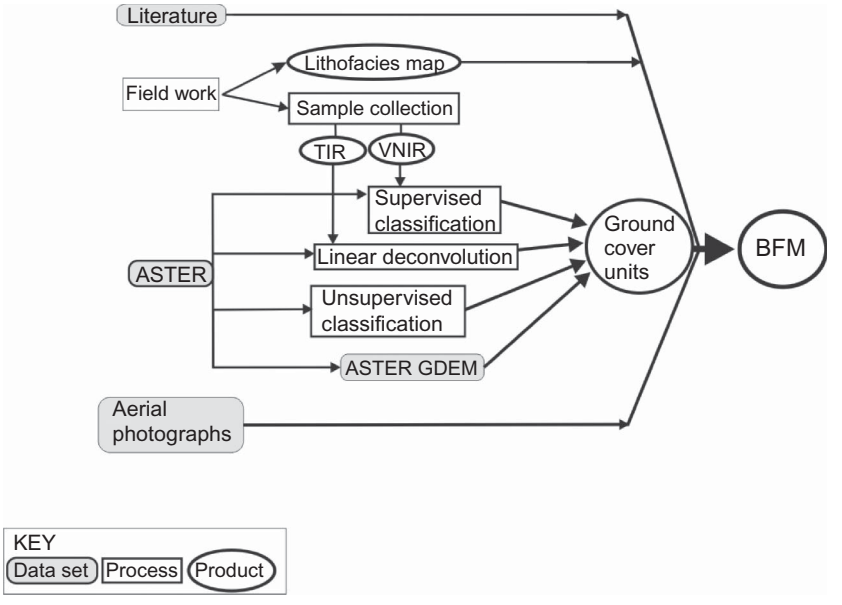

Figure 4. Flow chart showing the multiple techniques used to produce the BFM. The map is the product of a combination of products from multiple data sets and methods of processing remote-sensing data. Four inputs: ASTER data, aerial photographs, field work, and literature are required for the construction of this BFM. Ground cover units are initially defined by comparing the results of supervised and unsupervised processing of ASTER spectral data in conjunction with the ASTERGDEM. The boundaries of the ground cover units were further refined using existing data sets from the literature, field work-based lithofacies maps, and aerial photographs.

areas exceeding that of the spatial resolution of the ASTER instrument – 15 m plus); and (3) previous documentation in regional literature. Representative units included: glaciovolcanic subaqueously emplaced basaltic lavas (micro- and macro-porphyritic), subaqueous basaltic lapilli and ash tuff, Askja subaerial basaltic lava, Valðalða basaltic subaerial lava, Askja historic basalt (1920s), Askja historic pumice components (1875 pumice, obsidian, and lithics), Askja hydrothermally altered rhyolite, diamicton, and basaltic glass (intrusive chill margin) (Figure 5). Preexisting regional maps indicate the presence of subaerial and glaciovolcanic deposits likely similar to the end-members within the region surrounding Askja (Figure 3). Samples and field observations were used for petrologic characterization of the lithologies mentioned above. The lithofacies map produced by this field work was used for comparison with remote-sensing results.

2.1.2. VNIR spectra

Directional VNIR reflectance spectra of the end-member lithology samples were collected at the Image Visualization and Infrared Spectroscopy (IVIS) laboratory of the University of Pittsburgh using an Analytical Spectral Devices (ASD) FieldSpec HH spectrometer (0.35–1.1 μm spectral range). Spectra were collected using a full-spectrum lamp for illumination and calibrated against a Spectralon® plate. Whole rock samples with intact natural surfaces were used. No atmospheric control was made due to the short path length (~0.5 m) and limited atmospheric contamination in this wavelength region. These spectra were used to create a hyperspectral end-member VNIR (H-VNIR) library of the selected

Downloaded by [Michael Ramsey] at 16:35 18 July 2013

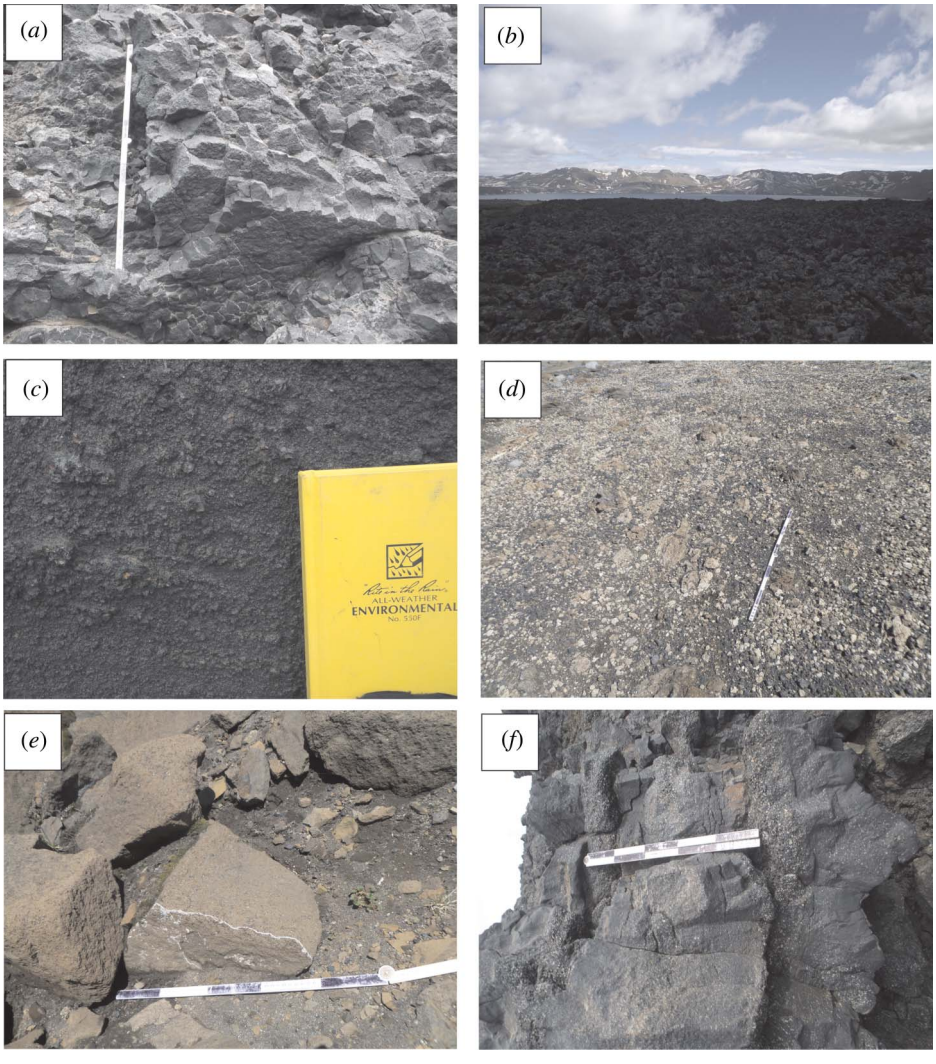

Figure 5. Field images of examples of lithologies selected for spectral end-members from Askja Volcano Iceland. (*a*) Glaciovolcanic pillow lava; (*b*) subaerial basaltic lava; (*c*) glaciovolcanic lapilli tuff; (*d*) 1875 rhyolitic pumice cover; (*e*) glaciovolcanic ash tuff; (*f*) subaqueous porphyritic lava.

lithologies. The spectra were also resampled by convolving them with the ASTER spectral response function to produce an ASTER spectral resolution end-member (A-VNIR) library (Figure 6). The visual and near infrared wavelengths were targeted to help highlight variations in the deposits based on colour, as significant variations were observed in the field and aerial photos correlating with the bimodal composition of eruptive products (rhyolitic pumice, basaltic lava).

2.1.3. TIR spectra

Hemispherical TIR emissivity spectra of the natural rock surfaces were also collected in the IVIS laboratory using a Nicolet Nexus 670 FTIR spectrometer with a KBr beam splitter and

Downloaded by [Michael Ramsey] at 16:35 18 July 2013

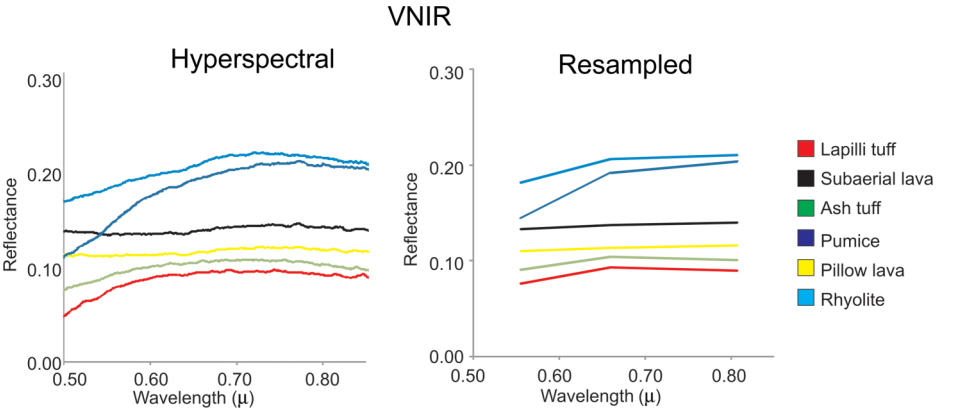

Figure 6. Selected VNIR hyperspectral and ASTER resolution reflectance spectra of representative end-member samples. The limited spectral diversity of the compositional units (lapilli tuff, subaerial lava, ash tuff, pumice, subaqueous lava, and rhyolite) is primarily from overall brightness levels of the samples. However, all units can be distinguished in the limited spectral resolution of ASTER.

Downloaded by [Michael Ramsey] at 16:35 18 July 2013

a DTGS detector (allowing data from 5 to 25 μm) (King et al. 2004; Carter et al. 2008). To derive the instrument response function, a two-temperature approach was used (Ruff et al. 1997). Samples were heated to 75°C and spectra were collected within an environment purged of CO_2 and H_2O to reduce atmospheric interference in this wavelength region. These spectra were used to create a hyperspectral end-member TIR (H-TIR) library. The spectra were also resampled by convolving them with the ASTER spectral response function to produce an ASTER spectral resolution end-member (A-TIR) library (Figure 7). The A-TIR end-member spectra were later used for linear deconvolution (Ramsey and Christensen 1998; Byrnes, Ramsey, and Crown 2004) to derive compositional and mineralogical information about the surface. TIR wavelengths are critical to mineralogical remote-sensing techniques as these wavelengths have clear atmospheric windows that correspond to important absorption features in silicate minerals.

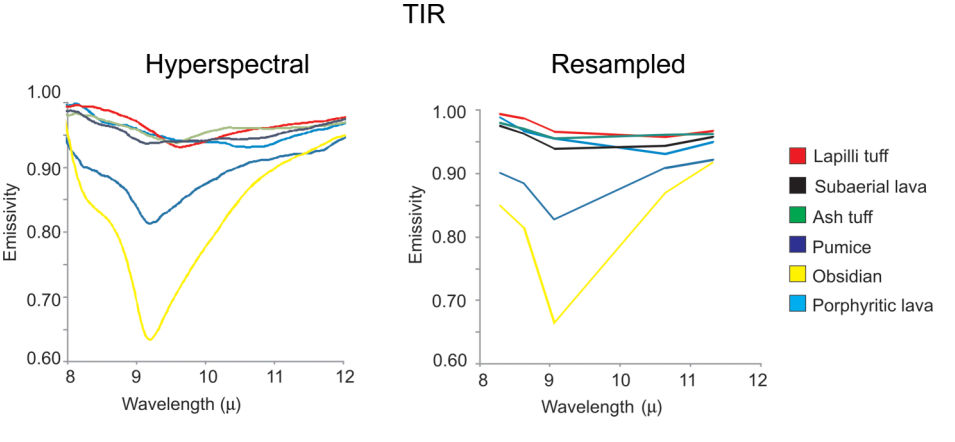

Figure 7. Selected TIR hyperspectral and ASTER resampled emissivity spectra of representative lithology samples (subaerial lava, ash tuff, lapilli tuff, pumice, obsidian, and porphyritic lava). TIR exhibits much more spectral diversity due to the primary Si-O vibrational frequency in all silicate samples.

2.2. Data processing

2.2.1. ASTER classification

VNIR, TIR, and combined VNIR/TIRASTER registered radiance data were classified using Iterative Self-Organizing Data Analysis Technique (ISODATA) (Ball and Hall 1965) and k-means (Lloyd 1982) algorithms. These unsupervised classifications are useful to highlight spectral variability within the scene (Figures 8 (*a*)–(*c*)). ISODATA differs from k-means in that the number of clusters is permitted to vary during classification. Classifications were set to use five initial classes, ten maximum classes, and ten iterations for ISODATA, and five classes for k-means.

Regions of interest (ROIs) selected from the field data, aerial photos, and the k-means classification results were then defined. Based on the compiled maps (lithofacies and regional), areas of known lithology were utilized for the creation of nine ROIs: 1875 pumice, subaqueous ash and lapilli tuff (fragmental glaciovolcanics), subaqueous pillow lavas (coherent glaciovolcanics), rhyolite lava, historical subaerial lava, weathered subaerial shield volcano lavas (Valðalða), water, snow, and vegetation. Supervised minimum-distance classifications were conducted using these ROIs on the ASTERVNIR reflectance data.

A similar process was used for the TIR emissivity data. End-members to be used in the TIR data were selected using the highest-resolution data sets, including the ASTERVNIR

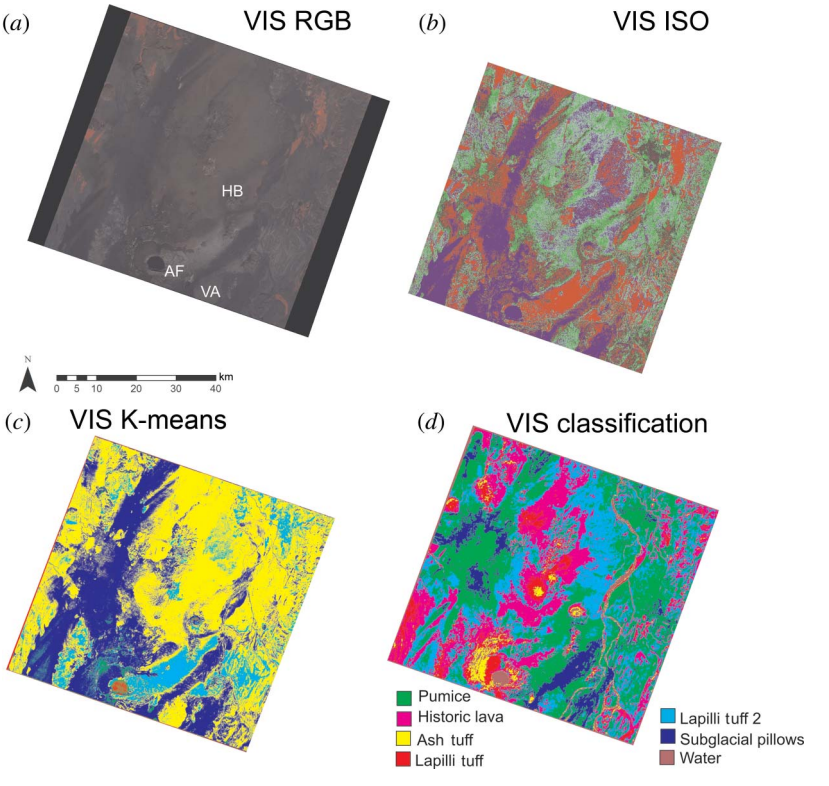

Figure 8. Example outputs of ASTERVNIR. (*a*) RGB image of bands 3, 2, and 1; (*b*) unsupervised ISO classification of VNIR wavelengths; (*c*) unsupervised k-means classification of VNIR using five breaks; (*d*) supervised classification of VNIR spectra using ROI defined from known field localities of major rock types.

Downloaded by [Michael Ramsey] at 16:35 18 July 2013

data, field data, and aerial photographs. Classes whose members exhibited spatial distributions smaller than a single TIR pixel (vegetation and snow) were excluded, due to lack of a pure end-member spectra within the ASTER data. The image-based end-members were used to create another spectral library (R-TIR), and then for further refinement of the minimum-distance classification.

2.2.2. VNIR reflectance spectra classification

The A-VNIR spectral library was used for supervised minimum-distance classification of the reflectance data. The 12-sample spectral library was further refined by creating ROI-based spectra from a targeted region of the known 1875 pumice that was highlighted by the initial classification to produce the A-VNIR + spectral library. The classification was rerun to produce the best-fit VNIR classification of the pumice ground cover unit (Figure 8(*d*)).

2.2.3. Linear deconvolution of emissivity spectra (TIR)

Spectral deconvolution, or linear unmixing, is based on the principal that the TIR energy emitted or reflected from a surface containing multiple components (minerals, lithologies) is a linear combination of the energy emitted from each individual component in proportion to the end-member's surface abundance (Ramsey and Christensen 1998). Because this mixing is linear, it can be modelled using an end-member library and a least squares linear fit of the data in order to extract the surface composition percentages of each end-member for every pixel (Adams, Smith, and Gillespie 1989; Byrnes, Ramsey, and Crown 2004; Ramsey and Dehn 2004). Linear deconvolution was conducted using the two broadband TIR spectral libraries (R-TIR and A-TIR).

Spectral deconvolution of ASTERTIR data using the image end-members was performed using combinations of end-member spectra from the R-TIR spectral library. The TIRROIs were defined initially with VNIR data and the spectra extracted from the ASTER emissivity data resampled to the same pixel size (15 m) as the VNIR data to ensure accurate ROI perimeters. The deconvolution process was then run on the atmospherically corrected surface emissivity data. The process was repeated using the laboratory-based A-TIR spectral library (Figure 9).

The deconvolution process involved using four spectral end-members plus a blackbody spectrum for all iterations. Multiple iterations were performed for each spectral library with end-members selected to target deposits of interest: 1875 pumice, historical lava, Holocene lava, fragmental glaciovolcanic deposits (ash tuff and lapilli tuff), and coherent glaciovolcanic deposits (subaqueous lava flows). Results were evaluated by examining the end-member images as well as the root-mean-squared (RMS) error images that map the success of fit of those end-members. This comparison allowed each spectral subset to be assessed, and to isolate false identifications of ground cover units in outlying areas, particularly the glaciovolcanic and pumice ground cover units.

2.3. Compilation of the best-fit map

Dominant ground cover units were identified from the ROI, VNIR, and TIR classifications as well as the linear deconvolution results. The ground cover units were then divided into sub-units based on the success and agreement of classifications and deconvolution results. Individual landforms were assessed independently, with the results from each methodology compared for consistency and extent of the units. The ground cover units

Downloaded by [Michael Ramsey] at 16:35 18 July 2013

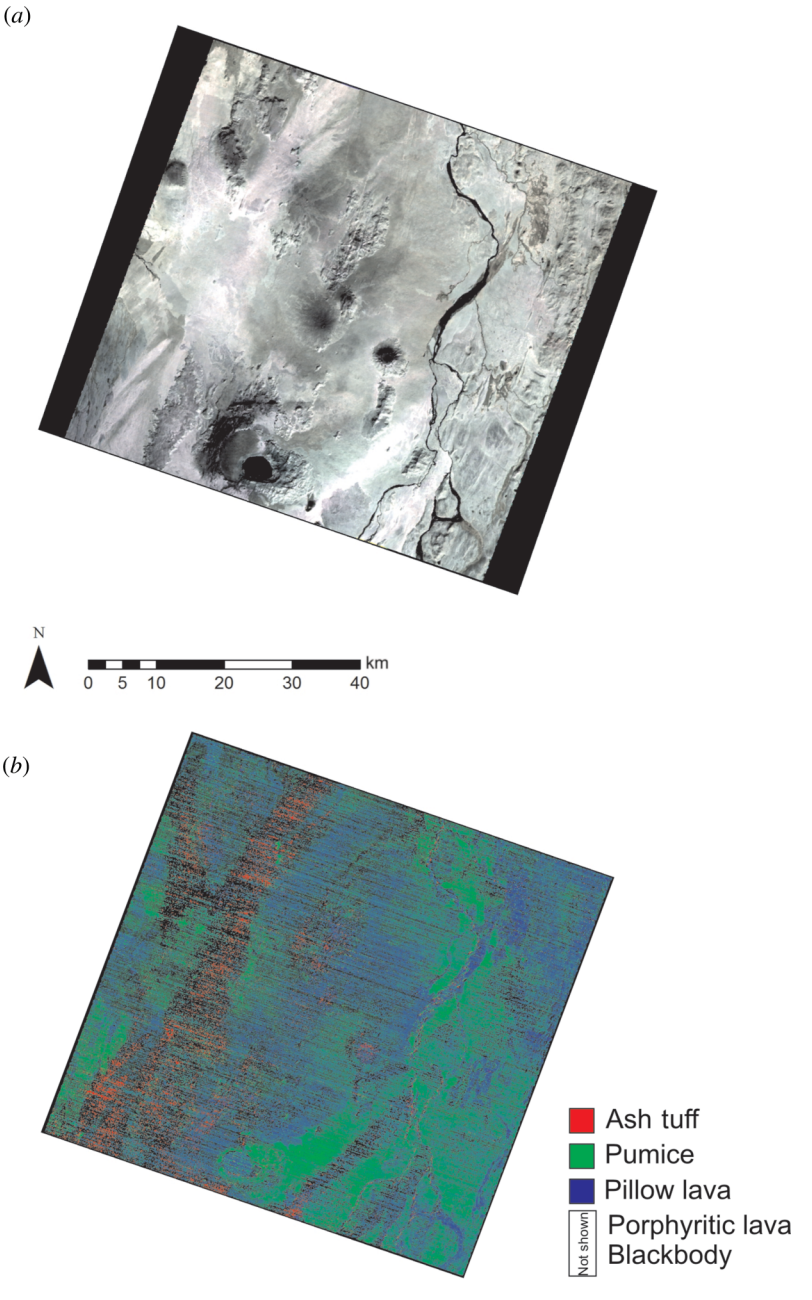

Figure 9. Thermal infrared ASTER outputs for the study area. (*a*) RGBTIR image using bands 14, 12, and 10, respectively; (*b*) example of linear deconvolution output using ash tuff (R), pumice (G), pillow lava (B), porphyritic lava spectra, and a black body. Linear deconvolution allows only four end-members and a blackbody as dictated by the number of bands in the ASTER instrument. Multiple iterations of unmixing were compared to discriminate the boundaries of the numerous ground cover units in the field area.

Downloaded by [Michael Ramsey] at 16:35 18 July 2013

were also compared with the GDEM to better define the boundaries of the lithologic units and morphological features. The end-member map was refined and further validated by comparing it with the regional (Figure 3) and Askjalithologic (Figure 2) maps. Individual ground cover units were compared with existing literature discussing the regional features and deposit distributions. The boundaries for the ground cover units were digitized in ArcGIS based on overlays from the multiple remote-sensing techniques using areas of the highest agreement between methods. For example, the 1875 pumice extent was constrained by the work of Carey, Houghton, and Thordarson (2010), which documented 233 km^2 of pumice coverage, and thus significant outliers (i.e. to the west of the volcanic complex where no pumice was recorded) could be excluded. The final map derived from the remote-sensing data is described as the best-fit map (BFM) of ground cover units (Figure 10). The 1875 pumice unit was subtracted from the ground surface to produce a 'pumice-free' best-fit map to highlight glaciovolcanic lithologic variations.

The construction of a BFM from multiple techniques was intended to reduce the error associated with any of the individual remote sensing-based mapping techniques described

Downloaded by [Michael Ramsey] at 16:35 18 July 2013

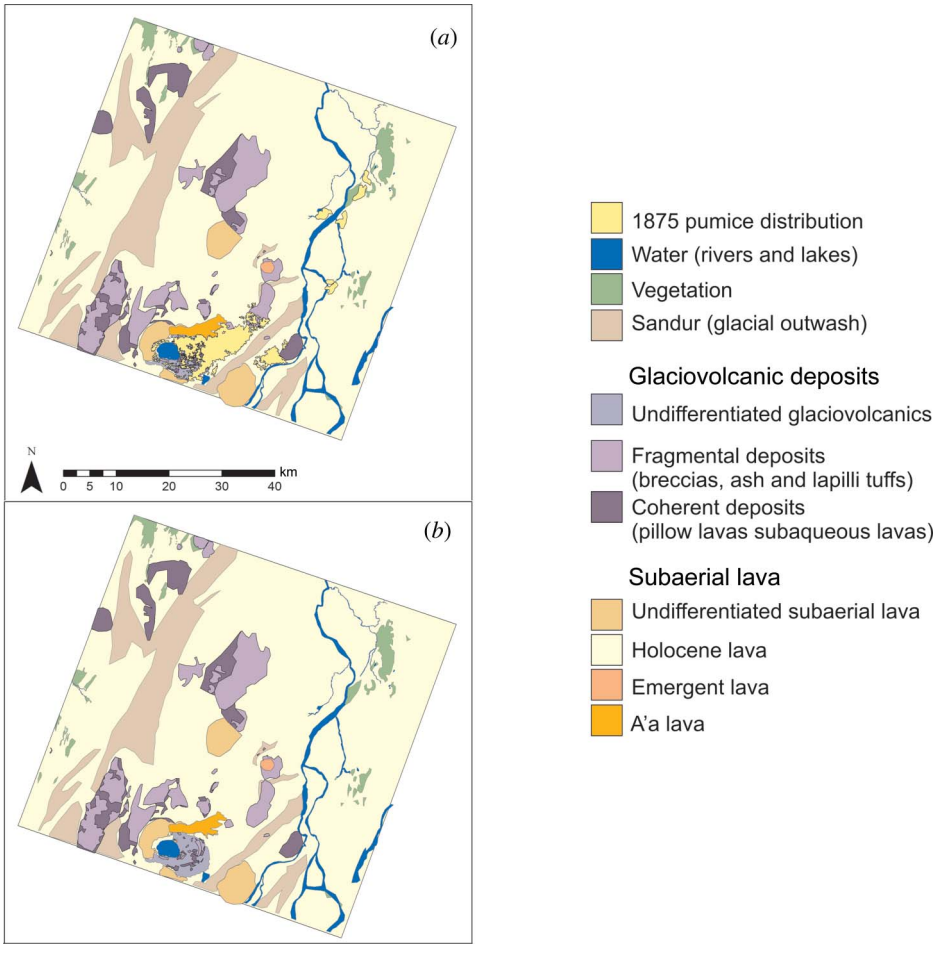

Figure 10. (*a*) Best-fit map (BFM) of ground cover units in the region north of Askja Volcano; (*b*) BFM with 1875 pumice removed.

here. By utilizing the lower spatial resolution but more lithologically diverse TIR data, and the high-spatial resolution but limited-spectral resolution VNIR data, the drawbacks of the individual techniques can be reduced. The results are further supported by the inclusion of the 25 m-resolution ASTERGDEM, which provides critical morphological data for interpreting unit boundaries and the distribution of topographically influenced fragmental deposits (e.g. sandur and pumice).

3. Results

3.1. Best-fit map

The BFM based on the ASTER data contains six primary ground cover units: subaerial lava (39%), sandur deposits (25%), glaciovolcanic deposits (21%), 1875 pumice (5%), water bodies (5%), and vegetation (4%). Two primary ground cover units, subaerial lava and glaciovolcanic deposits, were further divided into textural, or geomorphologically distinguished, sub-units. Subaerial lava was divided into four subgroups based on the level of detail identified through the mapping process: a'a lava, shield volcano, undifferentiated Holocene lava, and emergent glaciovolcanic. The a'a subgroup was defined by a high blackbody anomaly on lava flows from 1960 and 2.9 ka just north of Öskjuvatn (Annertz, Nilsson, and Sigvaldason 1985), a result of the high surface roughness of the flows (Ramsey and Fink 1997). This does not preclude the presence of other a'a flows; rather, it indicates the distinctive nature of these particular deposits. Shield volcano lavas, Holocenelava, and emergent lava were distinguished from one another by their geomorphic expression and relative elevation to the regional base elevation. Shield volcano lavas were distinguished by their distinctive low-angle relief and near circular morphologies and subaerial characterization by TIR deconvolution. These features cannot be assigned any age relationships using the remote techniques alone due to the similarity of the flows and aeolian cover. The Holocene lavas that infill the large Askja caldera were grouped with the shield volcano lava ground cover sub-unit due to their association with a single geomorphologic feature and distinctive quality relative to the Holocene lavas of the surrounding area. This assignment is intended to reflect morphology, not imply a genetic origin of the lavas. Emergent lavas are a unique product of glaciovolcanic complexes where subaqueous lavas and tuffs are capped by subaerial lavas. These lavas were identified as subaerial lavas that occur perched atop high topographic features, particularly subaqueous-dominated features, in this case Herðubreið glaciovolcanic volcano (Figure 10). The general base topography identified by TIR techniques as subaerial lava was mapped as undifferentiated Holocene lava, which is supported by regional mapping by Annertz, Nilsson, and Sigvaldason (1985) (Figure 3).

The glaciovolcanic deposits unit was divided into fragmental and coherent-dominated subgroups to reflect ash and lapilli tuffs from effusive pillow and sheet lavas. A third subgroup, porphyritic units, was attempted. Porphyritic deposits cover $>1\%$ of the field map, but the TIR spectral mapping identified only 3% of the mapped porphyritic units from the lithofacies map. As such, the training areas were determined to be inadequate for the identification for this level of detail relative to the two major glaciovolcanic subgroups. Fragmental glaciovolcanic deposits were distinguished from coherent units by their frequent misclassification as other clastic deposits (sandur and pumice) and correlation with laboratory VNIR and TIR spectra of the known fragmental deposits from Askja (dominantly ash tuff) (Table 1). Coherent glaciovolcanic deposits include subaqueous lavas of pillowed, lobate, and sheet morphologies and include common clast-rich breccias associated with the lavas. Based on the deposits mapped at Austurfjöll, the deposits are assumed to be dominated by pillowed lava flows.

Downloaded by [Michael Ramsey] at 16:35 18 July 2013

Table 1. Aerial extent of ground cover units in best-fit map (Figure 9), with comparison to existing aerial extent from the regional map (Figure 3).

	BFM		Regional map
Feature	m^2	% of total	m^2
Water	1.03×10^8	5	
Vegetation	8.41×10^7	4	
Pumice	1.11×10^8	5	2.33×10^8
Valðalða	5.99×10^7	3	4.53×10^7
Subaerial lava	1.18×10^8	6	
A'a lava	2.25×10^7	1	9.86×10^6
Shield volcanoes	3.18×10^7	1.5	2.40×10^8
Emergent lava	4.55×10^6	0.2	
Holocene lava (undifferentiated)	7.90×10^8	39	4.90×10^8
Sandur	5.06×10^8	25	
Glaciovolcanic	4.31×10^8	21	3.57×10^8
Fragmental	2.66×10^8	13	
Subaqueous lavas	2.89×10^8	14	

Downloaded by [Michael Ramsey] at 16:35 18 July 2013

Due to a combination of pumice cover, 1920s lava flow cover, and steep slopes, approximately 19% of the 49 km^2 glaciovolcanic deposits of Austurfjöll massif are exposed for satellite based ground-cover mapping (Figure 11(*a*)). The corridors of exposed glaciovolcanic deposits within the pumice unit are in the order of <1 km in width and up to 4 km long. A comparison of the DEM and pumice-free areas of Austurfjöll reveals a correlation of topographic highs with pumice-free regions of Austurfjöll (Figure 11(*b*)). An overlay of 1875 pumice on the lithofacies map shows the diversity of lithologic units exposed in areas not obscured by the pumice (Figure 11(*c*)). However, not all of the pumice-free areas were successfully discriminated between fragmental and coherent-dominated glaciovolcanic units using remote-sensing techniques (Figure 11(*d*)), and instead are classified as undifferentiated glaciovolcanic deposits (Figure 12). Of the viable surfaces on Austurfjöll massif, 66% of those surfaces are identified as coherent glaciovolcanic units.

A comparison of the various mapping techniques used to create each layer and the areal extent of the final units and any interim steps necessary is presented in Table 2. The overall distribution of glaciovolcanic units is larger in the BFM (17%) than the previous map, and the placement and extent of features farther from Askja have been improved by topographic data (Figure 12). However, small-scale features (exposures below the spatial resolution of the data) in the vicinity of the calderas were not consistently recognized by either the VNIR or TIR techniques, and thus do not appear on the BFM (Figure 12). The BFM also incorporates additional ground cover units that were discriminated in existing maps of the region (e.g. fragmental from coherent glaciovolcanic units, sandur, and vegetation).

Non-lithologic units (water and vegetation) comprise 9% of the scene. The water bodies are well correlated with recent maps of the major water features (Öskjuvatn, Jökulsá á Fjöllum, and Dyngjuvatn). Minor tributaries and ponding near the river are probably ephemeral or dynamic seasonally and annually, and thus the BFM is only representative of their condition in August 2010. The snow ground cover unit was dropped from

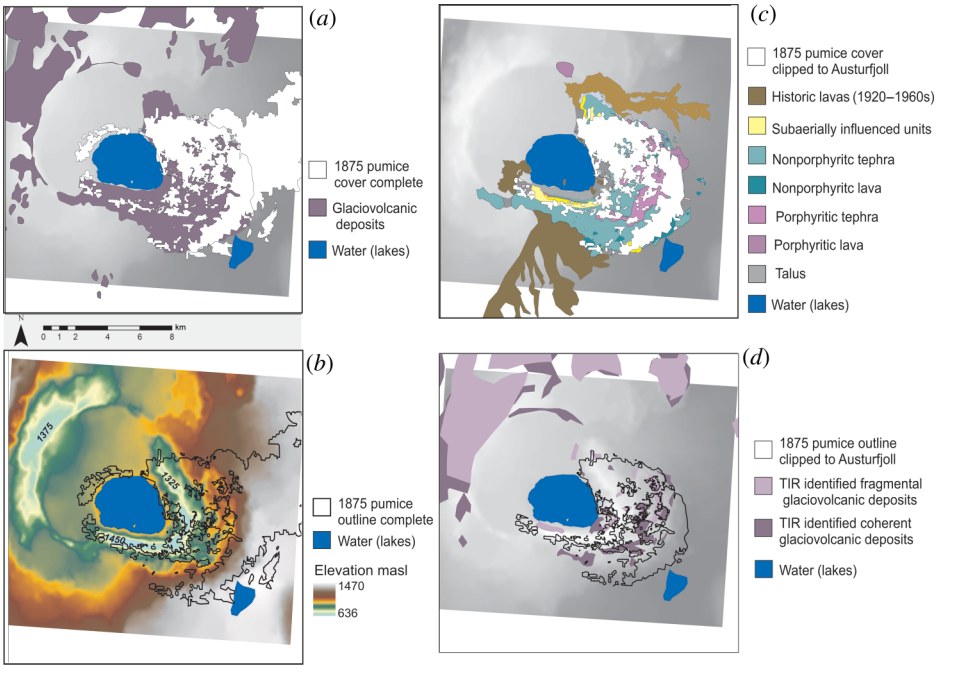

Figure 11. Distribution of the 1875 pumice proximal to the Austurfjöll massif overlain on a greyscale hillshade (derived from 10 m LoftmyndirDEM). (*a*) Complete 1875 distribution of the pumice overlapping the glaciovolcanic deposits. (*b*) Outline of the 1875 pumice over coloured hillshade to show the relationship between eroded pumice and the topography of the Austurfjöll massif. The pumice is mostly preserved in topographic lows. (*c*) 1875 pumice cropped to extent over Austurfjöll to show the exposure of lithology-mapped field units under the pumice. (*d*) Outline of cropped pumice distribution of TIR-based discrimination of glaciovolcanic units.

the final map due to its low spatial extent. Snow has a high degree of temporal variability and, for this particular scene, did not have sufficient training areas to create an accurate ROI.

4. Discussion

The BFM serves as a useful lithologic and ground cover map for the region surrounding Askja volcano because it (1) increased the aerial extent of the map of the portion of the Northern Volcanic Zone around Askja; (2) includes the new discrimination of two lithologic subgroups of glaciovolcanic massifs; (3) contains revised data on the distribution of the remobilized 1875 pumice deposit; and (4) introduces new ground cover units: sandur and vegetation. The production of the map served as a successful test for remote sensing-based mapping of glaciovolcanic terrains in Iceland, which has had a very limited application in the past. The features identified in the map are well constrained by topography and previous work, but they require more detailed work such as at Askja to establish proper geologic map units. The divisions established here serve the purpose of identifying a greater diversity in the landscape than previously noted and highlighting areas of unique composition, morphology, and texture relevant to volcanic and palaeoclimate reconstructions of the region.

Downloaded by [Michael Ramsey] at 16:35 18 July 2013

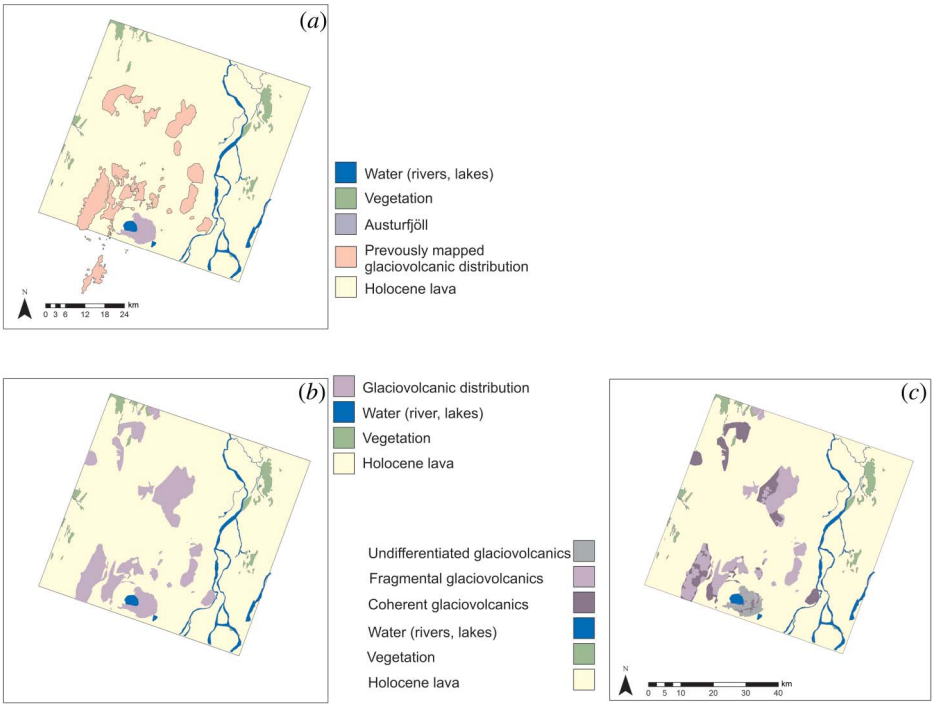

Figure 12. Comparison of glaciovolcanic unit distributions between existing maps (regional map Figure 3) and remote sensing based BFM with 1875 pumice and other ground cover units removed. (*a*) Glaciovolcanic units as compiled from the previous literature on Askja and surroundings (Hjartadottir et al. 2009; Annertz, Nilsson, and Sigvaldason 1985); (*b*) undifferentiated glaciovolcanic deposit distribution in BFM, results with constraints from ASTERGDEM topographic data; (*c*) differentiated glaciovolcanic deposits in BFM including fragmental, coherent, and undifferentiated glaciovolcanic deposits.

VNIR-based methodologies were successful at identifying vegetation, pumice, and sandur ground cover units. The VNIR also served as support for the identification of subaerial lava (and sub-units), and fragmental glaciovolcanic deposits. The high spatial resolution (15 m/pixel) of the VNIR data was necessary to discriminate detailed aspects of the vegetation and pumice. These units display high contrast in the visible wavelengths, producing well-defined units from both supervised and unsupervised classifications. The sandur ground cover unit represents only the thickest areas of glacial outwash, having a uniform colouration and texture that distinguish it from lava flow surfaces. However, there is significant aeolian action remobilizing the sand, and this map does not include dusting of outwash-derived aeolian sands that are encountered in the field as these are typically heterogeneous in distribution at a scale smaller than the spatial resolution of the data involved here.

Supervised VNIR classifications produced highly variable results, with the least consistent results produced using the laboratory-based hyperspectral end-member classification. The VNIR classifications were limited by the low brightness variability of the end-member samples. The glaciovolcanic deposits were all dark basaltic samples with high vesicularity and/or porosity. However, the unsupervised classifications were highly consistent and had a high correlation of external unit boundaries with TIR results, highlighting the same dominant fragmental groundcover features (sandur and pumice). Consequently, the

Downloaded by [Michael Ramsey] at 16:35 18 July 2013

Table 2. Techniques used to identify individual ground cover units.

	VIS				TIR				
Feature	False colour	ISO	ROI Class.	AVNIR Class.	ROI Class.	ROI Unmix	ATIR Unmix	Black-body	Topography
Water		X	X	X	X	X	X	X	
Vegetation	X		X						
Pumice	X	X	X	X	X	X	X		
Valðalða									X
Subaerial lava		X	X	X		X	X		
A'a lava								X	
Shield volcanoes									X
Emergent lava									X
Sandur	X	X	X	X	X	X	X		
Glacio-volcanic			X						X
Fragmental-dominated		X					X		
Subaqueous lavas						X	X		
Holocene lava (undifferenti-ated)		X	X	X	X	X			X

Downloaded by [Michael Ramsey] at 16:35 18 July 2013

unsupervised VNIR classifications were given the highest preference in map creation, followed by ROI-based end-member classifications and A-VNIR classification.

The remaining ground cover units were mapped based on variations in micron-scale roughness and composition identified in the TIR classifications and linear deconvolutions, with support from VNIR and topographic data. The glaciovolcanic deposits were most successfully identified using A-TIR and ROI spectral deconvolution (in that order). Thermal wavelength characteristics are primarily produced by the abundance of micron-scale roughness elements such as vesicles and macro-phenocrysts (Ramsey and Fink 1999; Byrnes, Ramsey, and Crown 2004). The textural qualities of the glaciovolcanic fragmental deposits and pillow lavas are distinct from the surrounding subaerial lava flows, but display large internal variability. The bulk of the fragmental deposits was identified using the linear deconvolution approach. Some deposits were more easily distinguished from coherent glaciovolcanic deposits with support from the VNIR, particularly Dyngjufjöll Ytri, where fragmental glaciovolcanics were identified by TIR spectral deconvolution as 1875 pumice (Sigvaldason 1992). This misclassification is the direct result of the textural similarity between the fragmental deposits of Dyngjufjöll Ytri and the 1875 pumice. Consequently, the two deposits are better distinguished by the unsupervised VNIR classification, which identifies the compositionally influenced colour variation between the basaltic glaciovolcanics and the rhyolitic pumice.

The glaciovolcanic deposits of Askja have the most complicated spectral signature of the edifices in the region. The massif has the greatest variability of all landforms in the map area. This variability is a result of the combination of extensive incision of the massif by erosion and caldera formation with resulting steep walls, and the abundance of more recent pumiceous deposits on the older (Pleistocene) deposits. Steep slopes on table mountains, like Herðubreið, and caldera walls, are not ideal targets for remote sensing as their steep slopes prevent the collection of spectra from glaciovolcanic units. In the case of

Herðubreið, only the emergent subaerial lava cap is recognized. Austurfjoll also has significant textural variability, as shown in the lithofacies map (Figure 2), including micro- and macro-porphyritic lavas and tuffs. It was anticipated that the macro-porphyritic lavas would have a distinct TIR spectral signature (Byrnes, Ramsey, and Crown 2004) (Figure 7). However, A-TIR linear deconvolution did not produce confident results. Additionally, the identification of units under the pumice by TIR remote-sensing techniques is less accurate due to the interference of 1875 pumice of thickness 0.05 to 2 m (Carey, Houghton, and Thordarson 2010). Nevertheless, interesting trends were produced on Austurfjöll; the areas identified successfully beneath the fringes of pumice deposits as coherent have high correlation, although limited direct overlap, with porphyritic units of the lithofacies map (Figure 11). The interference of the pumice may have led to the misidentification of porphyritic tephra and lava as coherent micro-porphyritic glaciovolcanic deposits. Therefore, distinction between coherent glaciovolcanic lavas that are micro- and macro-porphyritic requires further investigation, whether remotely or in the field.

Subaerial lavas as a group were spectrally unique, with consistent results between classification and deconvolution techniques. The establishment of the subgroups was enabled by incorporating the topographic data. This was of particular importance for distinguishing between shield volcanoes and background Holocene lava. These two subgroups do not have significant compositional, textural, or visible colour variations as revealed in the TIR and VNIR spectra. This lack of spectral variation is unexpected, as the shield volcano Valðalða is interglacial in age and has significant glacial scour, but remains indistinguishable compositionally from the background Holocene lava in the TIR. The similarity of the scoured Valðalða and Holocene lava is likely due to the dominance of pahoehoe flows in both subgroups and thin aeolian cover (derived from the sandur) over both features, muting surface textures. This highlights the continued need for familiarity with regions with as much complexity as that around Askja, and the benefit of incorporating spectral, topographic, and ground-based investigations. The DEM was utilized to identify the discrete morphologies of Valðalða and Kollóttadyngja shield volcanoes, which enabled the separation of these features from the Holocene lava subgroup. The remaining shields indicated in the regional map (Figure 3) have much less topographic relief, and were not identified through this mapping process; they are instead included in the Holocene lava subgroup.

Unconsolidated fragmental ground cover units (such as pumice and sandur) should also be easily resolved using thermophysical techniques such as apparent thermal inertia (Scheidt, Ramsey, and Lancaster 2010); however, the high latitude, generally cloudy weather, and long snowy season in the Icelandic Highlands has, to date, precluded the acquisition of an ASTER day–night pair of images over Askja necessary for this technique. It would be worthwhile to consider the testing of apparent thermal inertia to detect unconsolidated fragmental ground cover units using other instruments with higher temporal resolution or ASTER data of regions with a higher abundance of useful scenes. The addition of higher spectral and spatial resolution data sets would also improve the discrimination of smaller or more compositionally mixed features.

5. Conclusions

The success of the best-fit map to reveal the diversity in textural and compositional units using only one ASTER data scene reveals the potential for regional mapping of glaciovolcanic terrains remotely. The variability observed within the glaciovolcanic massifs surrounding Askja volcano warrants further field investigation in order to better understand the volcanic and depositional processes, as well as the regional volcanic evolution

Downloaded by [Michael Ramsey] at 16:35 18 July 2013

and glacial history of the NVZ in Iceland. Existing maps of this and other volcanic zones in Iceland do not highlight the diversity of lithofacies at glaciovolcanic centres, which belies the nature of the evolution of these volcanic systems. Remotely produced ground cover maps can serve as an important starting point for regional mapping and the identification of future study sites for volcanic and palaeoclimate research in Iceland and other difficult terrains such as British Columbia and Antarctica (Figure 12). The glaciovolcanic deposits of these regions are becoming increasingly important due to the lack of preservation of other terrestrial palaeoclimate indicators, particularly of pre-last glacial maximum ice positions (Bourgeois, Daeuteuil, and Van Vliet-Lanoë 2000; Edwards et al. 2009; Edwards, Russel, and Simpson 2011). This technique successfully identified two major textural units of glaciovolcanic deposit types. These subunits represent very different eruption styles and thermodynamic histories, and consequently the impact of each eruption on the overlying ice sheet. Furthermore, this technique helps locate coherent lava facies, which are required for the most successful dating techniques for volcanic rocks, and necessary for producing rigorous palaeoclimate proxies such as ice thickness records. Remote investigations such as this may provide good candidates for further research and chronologies of the region and help focus future field work.

This project successfully validated remote-sensing data through the use of existing and recently collected data, but it also revealed the potential for supplementing field-based mapping, particularly of remobilized deposits and ground cover units. The new outline of the remobilized 1875 pumice distribution over the Austurfjöll massif adds a highly visible, but previously poorly constrained, unit to the lithologic map (Figure 11(*c*)). With over one decade of global ASTER data, this study provides another successful application of integrated ASTERVNIR and TIR data for complex compositional reconnaissance mapping of volcanic terrains around the world. While Iceland's latitude provided a greater opportunity for satellite overpasses, snow and ice cover prevent the collection of useful scenes. Other locations may have a richer archive for this approach due to more favourable climate. Additionally, as the TIR was only one component of this work, other satellites, such as the Landsat series, including the recently launched LDCM, may provide further opportunities for the refinement of this work and its applications to high-latitude glaciovolcanic centres despite their relative lack of TIR bands.

Downloaded by [Michael Ramsey] at 16:35 18 July 2013

Acknowledgements

Field work logistics were made possible by the Vatnajökull National Park Iceland, the University of Iceland, and a NSF grant to IPS. ASTER global DEM is a product of METI and NASA. The manuscript was improved by two anonymous reviewers.

References

Adams, J. B., M. O. Smith, and A. R. Gillespie. 1989. "Simple Models for Complex Natural Surfaces: A Strategey for the Hyperspectral Era of Remote Sensing." *IGARSS Canadian Symposion of Remote Sensing* 12: 16–21.

Annertz, K., M. Nilsson, and G. E. Sigvaldason. 1985. *The Postglacial History of Dyngjufjöll*. Nordic Volcanological Institute Report 8503, 1– 22. Reykjavik: Nordic Volcanological Institute.

Ball, G., and D. Hall. 1965. "Isodata, a Novel Method of Data Analysis and Pattern Classifcation." *Standford Research Institute Technical Report* 79, 61 pp.

Bemmelen, R. W. V., and M. G. Rutten. 1955. *Tablemountains of Northern Iceland: (and Related Geological Notes)*. Leiden: E.J. Brill.

Bourgeois, O., O. Daeuteuil, and B. Van Vliet-Lanoë. 2000. "Geothermal Control on Flow Patterns in the Last Glacial Maximum Ice Sheet of Iceland." *Earth Surface Processes and Landforms* 25: 59–76.

Byrnes, J. M., M. S. Ramsey, and D. A. Crown. 2004. "Surface Unit Characterization of the Mauna UluFlow Field, Kilauea Volcano, Hawai'i, Using Integrated Field and Remote Sensing Analyses." *Journal of Volcanology and Geothermal Research* 135: 169–193.

Carey, R. J., B. F. Houghton, and T. Thordarson. 2009. "Abrupt Shifts Between Wet and Dry Phases of the 1875 Eruption of Askja Volcano: Microscopic Evidence for Macroscopic Dynamics." *Journal of Volcanology and Geothermal Research* 184: 256–270.

Carey, R. J., B. F. Houghton, and T. Thordarson. 2010. "Tephra Dispersal and Eruption Dynamics of Wet and Dry Phases of the 1875 Eruption of Askja Volcano, Iceland." *Bulletin of Volcanology* 72: 259–278.

Carter, A. J., O. Girina, M. S. Ramsey, and Y. V. Demyanchuk. 2008. "ASTER and Field Observations of the 24 December 2006 Eruption of Bezymianny Volcano, Russia." *Remote Sensing of the Environment* 112: 2569–2577.

Edwards, B. R., J. K. Russel, and K. Simpson. 2011. "Volcanology and Petrology of Mathews Tuya, Northern British Columbia, Canada: Glaciovolcanic Constraints on Interpretations of the 0.730 Ma Cordilleran Paleoclimate." *Bulletin of Volcanology* 73: 479–496.

Edwards, B. R, I. P. Skilling, B. Cameron, C. Haynes, A. Lloyd, and J. H. D. Hungerford. 2009. "Evolution of an Englacial Volcanic Ridge: Pillow Ridge Tindar, Mount Edziza Volcanic Complex, NCVP, British Columbia, Canada." *Journal of Volcanology and Geothermal Research* 185: 251–275.

Graettinger, A. H. 2012. "Building Ice-Age Askja, Iceland: Products, Processes, and Paleoclimate." In *Geology and Planetary Science*, 462 pp. Pittsburgh: University of Pittsburgh.

Hjartardóttir, A. R., P. Einarsson, and H. Sigurdsson. 2009. "The Fissure Swarm of the Askja Volcanic System Along the Divergent Plate Boundary of N Icealand." *Bulletin of Volcanology* 71: 961–971.

Höskuldsson, Á. 1987. *Some Chemcial Properties of the Askja Volcanic Center*, 117–138. Reykjavik: Nordic Volcanological Institute, University of Iceland.

Jakobsson, S. P., K. Jónasson, and I. A. Sigurdsson. 2008. "The Three Igneous Rock Series of Iceland." *Jökull* 58: 117–138.

King, P. L., M. S. Ramsey, P. F. McMillian, and G. A. Swayze. 2004. "Laboratory Fourier Transform Infrared Spectroscopy Methods for Geologic Samples." In *Infrared Spectroscopy in Geochemsitry, Exploration Geochemistry, and Remote Sensing*, edited by P. L. King, 57–911. London, ON: Mineralogical Association of Canada.

Kuritani, T., T. Yokoyama, H. Kitagawa, K. Kobayashi, and E. Nakamura. 2011. "Geochemical Evolution of Historical Lavas From Askja Volcano, Iceland: Implications for Mechanisms and Timescales of Mamgmatic Differentiation." *Geochemica Et Cosmochimica Acta* 75: 570–587.

Lloyd, S. P. 1982. "Least Squares Quantization in PCM." *IEEE Transactions on Information Theory* 28: 129–137.

Ramsey, M. S., and P. R. Christensen. 1998. "Mineral Abundance Determination: Quantitative Deconvolution of Thermal Emission Spectra." *Journal of Geophysical Research* 103: 577–596.

Ramsey, M. S., and J. Dehn. 2004. "Spaceborne Observations of the 2000 Bezymianny, Kamchatka Eruption: The Integration of High-Resolution ASTER Data Into Near Real-Time Monitoring Using AVHRR." *Journal of Volcanology and Geothermal Research* 135: 127–146.

Ramsey, M. S., and J. Fink. 1997. "Mapping Vesicularity of Hawaiian Lava Flows Via Thermal Infrared Remote Sensing." *American Geophysical Union EOS Transactions* 78 (46): F777.

Ramsey, M. S., and J. Fink. 1999. "Estimating Silicic Lava Vesicularity with Thermal Remote Sensing: A New Technique for Volcanic Mapping and Monitoring." *Bulletin of Volcanology* 61: 32–39.

Ruff, S., P. R. Christensen, P. W. Barbera, and D. L. Anderson. 1997. "Quantitiative Thermal Emission Spectroscopy of Minerals: A Laboratory Technique for Measurement and Calibration." *Journal of Geophysical Research* 102: 14899–14913.

Scheidt, S., M. S. Ramsey, and N. Lancaster. 2010. "Determining Soil Moisture and Sediment Availability at White Sands DUne Field, NM From Apparent Thermal Intertia (ATI) Data." *Journal of Geophysical Research* 115: F0204109.

Schopka, H. H., M. T. Gudmundsson, and H. Tuffen. 2006. "The Formation of Helgafell, Southwest Iceland, a Monogenetic Subglacial Hyaloclastite Ridge: Sedimentology, Hydrology and Volcano-Ice Interaction." *Journal of Volcanology and Geothermal Research* 152: 359–377.

Sigurdsson, H., and R. Sparks. 1978. "Rifting Episode in North Iceland in 1874–1875 and the Eruptions of Askja and Sveinagja." *Bulletin of Volcanology* 41: 149–167.

Downloaded by [Michael Ramsey] at 16:35 18 July 2013

Sigvaldason, G. E. 1964. “Some Geochemical and Hydrothermal Aspects of the 1961 Askja Eruption.” *Contributions to Mineralogy and Petrology* 10: 263–274.
Sigvaldason, G. E. 1968. “Structure and Products of Subaquatic Volcanoes in Iceland.” *Contributions to Mineralogy and Petrology* 18: 1–16.
Sigvaldason, G. E. 1992. “Recent Hydrothermal Explosion Craters in an Old Hyaloclastite Flow, Central Iceland.” *Journal of Volcanology and Geothermal Research* 54: 53–63.
Sigvaldason, G. E. 2002. “Volcanic and Tectonic Processes Coinciding with Glaciation and Crustal Rebound: An Early Holocene Rhyolitic Eruption in the Dyngjufjöll Volcanic Centre and the Formation of the Askja Caldera, North Iceland.” *Bulletin of Volcanology* 64: 192–205.
Thorarinsson, S., and G. Sigvaldason. 1962. “The Eruption in Askja, 1961 a Preliminary Report.” *American Journal of Science* 260: 641–651.
Thoroddsen, T. 1925. *Die Geschichte Der IslandischenVulkane*. Copenhagen: Royal Academy of Sciences and Letters.
Werner, R., and H.-U. Schmincke. 1999. “Englacial Vs Lacustrine Origin of Volcanic Table Mountains: Evidence From Iceland.” *Bulletin of Volcanology* 60: 335–354.
Werner, R., H.-U. Schmincke, and G. E. Sigvaldason. 1996. “A New Model for the Evolution of Table Mountains: Volcanological and Petrological Evidence From Herdubreid and Herdubreidartögl Volcanoes (Iceland).” *GeolRundsch* 85: 390–397.
Þorarinsson, S. 1963. *Elduríöskju*. Reykjavik: Almenna Bókafélagið.

Downloaded by [Michael Ramsey] at 16:35 18 July 2013